



PERGAMON

Journal of Quantitative Spectroscopy &
Radiative Transfer 65 (2000) 135–149

Journal of
Quantitative
Spectroscopy &
Radiative
Transfer

www.elsevier.com/locate/jqsrt

Statistical fitting analysis of Stark-broadened optically thick Ar II spectra measured in ion beam transport experiments

Hyun-Kyung Chung^{a,*}, David H. Cohen^{b,c}, Joseph J. MacFarlane^b,
James E. Bailey^d, Ping Wang^b, Gregory A. Moses^e

^aHarvard-Smithsonian Center for Astrophysics, MS-14, 60 Garden St., Cambridge, MA 02138, USA

^bPrism Computational Sciences, 16 N. Carroll St., Madison, WI 53703, USA

^cBartol Research Institute, University of Delaware, Newark, DE 19711, USA

^dSandia National Laboratory, P.O. Box 5800, Albuquerque, NM 87185, USA

^eFusion Technology Institute, University of Wisconsin, 1500 Engineering Dr., Madison, WI 53706, USA

Abstract

We present a method for fitting a multi-line spectrum with an emission model that accounts for multiple line-broadening mechanisms and the effects of finite optical depth. This technique includes an analysis of the joint-probability distribution of the model parameters that allows one to determine statistically valid confidence limits on the fitted parameters. We apply this method to a time series of optical Ar II spectra produced when an intense lithium beam (kinetic energy of 9 MeV and current density of 22 kA cm^{-2}) was injected into an argon gas cell. We show that line optical depth effects are important in these data, and by including finite optical depth as well as Stark and Doppler broadening in the model-fitting procedure, we are able to place meaningful constraints on the time-dependent Ar II level populations and the electron density in the gas cell. The values we derive for these quantities are in reasonably good agreement with detailed collisional-radiative models that include the effects of non-thermal electrons and beam ions. Understanding the time-dependent conditions in the gas cell is critical for efficient beam transport. © 2000 Elsevier Science Ltd. All rights reserved.

1. Introduction

The broadening of spectral emission lines has the potential to provide a significant amount of information about the physical conditions of plasmas. Opacity effects, however, can introduce considerable uncertainty into such an analysis by substantially complicating the observed line

* Corresponding author. Tel.: 001-617-496-7611; fax: 001-617-496-7668.

E-mail address: hchung@cfa.harvard.edu (H.-K. Chung)

shapes. In such a situation, the total broadening of optically thick lines will be affected by a combination of opacity effects and broadening mechanisms inherent to the plasma (e.g. Stark and Doppler). We note that opacity effects include modifications to line intensities as well as to line widths. Determining the relative contributions of Stark broadening and optical depth effects is a common focus of plasma spectroscopy (see for example, Ref. [1]). Theoretical profiles for optically thick lines in which Stark broadening is important have been calculated [2], but determining the contribution of one mechanism without a priori knowledge of the other is problematic. However, using multi-line spectral data, in which some lines are optically thick and others are not, a statistical model-fitting analysis can be employed to disentangle Stark broadening and opacity effects. In this way, information can be derived about both the electron density (via the Stark broadening) and the level populations (via the opacity) in the emitting plasma. Furthermore, such a statistical fitting analysis allows one to place formal uncertainties on the model parameters of interest. These uncertainties can often be quite small due to their dependence on data from numerous spectral lines.

We apply this analysis to Ar II optical spectra obtained during ion beam transport experiments in an argon gas cell on the particle beam fusion accelerator (PBFA-II) at Sandia National Laboratory [3]. Stark broadening dominates the optically thin emission lines in these spectra, but it is expected that the strongest lines may be quite optically thick. Indeed, fitting optically thin Voigt profiles to these lines individually yields widely divergent values for the electron density among the different lines, and in general radically overestimates the mean charge state of the argon plasma. In this paper we show how to provide meaningful constraints on the electron density and line opacities in the argon gas cell plasma by employing a spectral model that includes optical depth and Stark-broadened effects in a joint probability distribution formalism. The model fitting and statistical analysis we describe and apply to the gas cell data in this paper are applicable in general to multi-line spectra in which broadening due to finite opacity acts in combination with other broadening mechanisms.

In Section 2 we briefly describe the ion beam transport experiments. The spectral model and statistical fitting analysis are described in Section 3. In Section 4 we discuss the results of our model fitting to the gas cell data, and conclude with a summary in Section 5.

2. Ion beam transport experimental spectra

High-intensity lithium ion beam experiments have been carried out at the particle beam fusion accelerator II (PBFA-II) facility at Sandia National Laboratory in order to investigate the potential for light ion beam inertial fusion [3,4]. A key element of ion fusion is beam transport from the final focusing apparatus to the target. To prevent beam disruption the beam is injected into a gas cell creating ionization that provides charge and current neutralization. With this method, understanding and control over the ionization processes which determine the transport plasma conductivity are essential. The work described here contributes to that understanding by measuring the time-dependent electron density and the bound-bound transition opacities in a beam intensity regime similar to the expected parameters for high yield fusion. In these experiments, a Li^+ beam is accelerated radially inward by a cylindrically symmetric applied magnetic field ion diode powered by the PBFA-II accelerator. The beam is transported through a 2 Torr argon gas

cell, where it is stripped to Li^{+3} and is then delivered to the target 13 cm away, located on the cylindrical axis. A schematic of the experimental set-up is shown in Fig. 1.

The peak kinetic energy and current density of the beam are 9 MeV and 22 kA cm^{-2} , respectively, at the spectrometer line of sight, and the duration of the beam pulse is 20 ns FWHM . Diagnosing the conditions in the gas cell is accomplished by acquiring high-resolution spectra from highly excited singly ionized argon (Ar II) measured with a fiber-coupled time-resolved spectrograph. The spectrograph line of sight is parallel to, and located 4 cm from, the cylindrical axis, as shown in Fig. 1. The data we report on here cover the range $4330\text{--}4380 \text{ \AA}$, with a spectral resolution of 0.5 \AA and an effective time resolution of 3 ns .

The Ar II lines that are included in the analysis are listed in Table 1, and a partial energy level diagram is shown in Fig. 2. In the argon gas cell, atomic processes are largely collisionally driven, with excitation and ionization due to three types of particles: the high-energy beam ions, non-thermal electrons that have been accelerated by interactions with the beam ions or large electric fields associated with the intense beam, and thermal electrons. Detailed time-dependent numerical simulations including these processes show that the argon atoms in the gas cell rapidly become singly and doubly ionized, with many excited levels having significant populations during portions

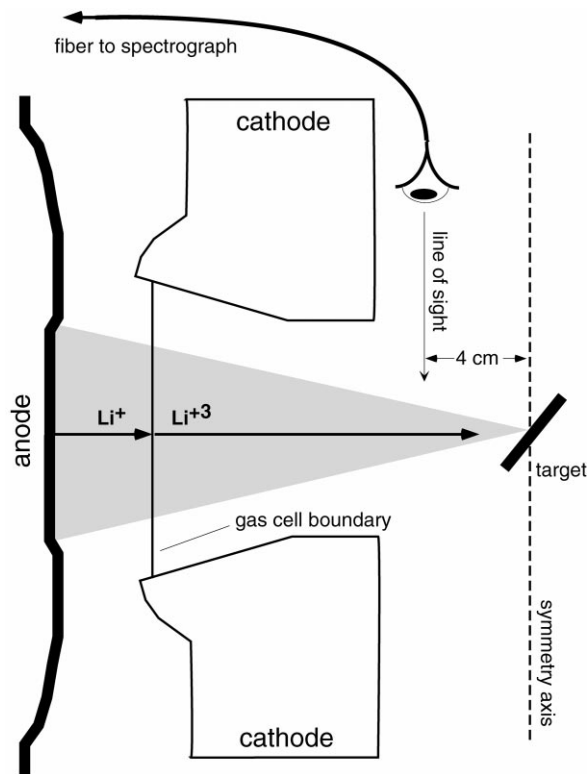


Fig. 1. A schematic representation of the ion beam transport experiments in the PBFA-II argon gas cell. Note that the spectrograph line of sight is perpendicular to the Li ion beam, and displaced about 4 cm from the target, which is on the cylindrical axis of the gas cell.

Table 1
Ar II lines used in the analysis

Wavelength (Å)	Lower level ^a	ΔE_1^b (eV)	Upper level ^a	ΔE_u^b (eV)	f -value ^c	gf	Stark Width ^d (Å)
4331.2 ^e	4s ⁴ P _{3/2}	16.75	4p ⁴ D _{3/2}	19.61	0.166	0.664	0.338
4332.0 ^e	3d ⁴ D _{3/2}	16.44	4p ⁴ P _{1/2}	19.31	0.023	0.092	0.320
4337.1	4p ² P _{1/2}	21.43	5s ² D _{3/2}	24.29	0.065	0.260	0.780
4348.1	4s ⁴ P _{5/2}	16.64	4p ⁴ D _{7/2}	19.50	0.483	2.898	0.292
4352.2	3d ⁴ D _{1/2}	16.46	4p ⁴ P _{1/2}	19.31	0.058	0.116	0.350
4362.1	3d ² D _{3/2}	18.66	4p ² D _{5/2}	21.50	0.026	0.104	0.320
4370.8 ^f	3d ² D _{3/2}	18.66	4p ² D _{3/2}	21.49	0.196	0.784	0.320
4371.3 ^f	3d ⁴ D _{5/2}	16.43	4p ⁴ P _{3/2}	19.26	0.041	0.246	0.323
4374.9	4p ² P _{3/2}	19.87	5s ² P _{3/2}	22.70	0.047	0.188	0.840
4376.0	4s ² P _{3/2}	17.14	4p ² S _{1/2}	19.97	0.030	0.120	0.244
4379.7	4s ⁴ P _{1/2}	16.81	4p ⁴ D _{1/2}	19.64	0.307	0.614	0.316

^aThe unprimed configurations have a ³P core and the primed configurations have a ¹D core.

^bEnergy above the Ar II ground state.

^cThe f -values are from Ref. [6].

^dThe Stark widths are from Ref. [7], and are scaled from the values tabulated there for $n_e = 10^{17} \text{ cm}^{-3}$. Where no values are found in the literature for a given line, we adopt 0.32 Å for lines with upper levels having $n = 4$. For the 4337 and 4375 Å lines, which arise from the $n = 5$ level and also do not have published Stark widths, we adopt the values from Ref. [7] for other Ar II transitions that have the same upper terms (3926 Å in the case of 4337 and 4219 Å in the case of 4375 Å.)

^{e,f} These line pairs are partially blended in the data.

of the beam pulse. These Ar II excited levels are initially populated directly from the Ar I ground state via knock-on collisions with non-thermal particles [5]. These calculations indicate that the absolute population densities of Ar II excited levels participating in the optical transitions can be sufficient to produce moderate to large optical depths ($\tau \gtrsim 10$ for the thickest lines). The associated opacity broadening must therefore be incorporated into the data analysis in order to accurately determine the plasma properties.

3. Model fitting procedure

In this section we will provide an operational description of the model fitting. The general procedure is to calculate a series of synthetic spectra, varying the free parameters each time, and then compare each model spectrum to the data. A goodness-of-fit statistic (we use χ^2) is minimized in order to determine the best-fit parameters. After this set of parameter values is determined, the χ^2 statistic is again used to place formal uncertainties on the data. The individual models are calculated by assuming a value for the electron temperature that is consistent with prior analyses [3,5], and further assuming that LTE among the excited states holds. The relative optical depths of the lines are thus fixed so that the depth of a single line specifies the optical depths of all the lines. Line profiles are then calculated based on the value of the (adjustable) optical depth parameter, and the (adjustable) electron density parameter.

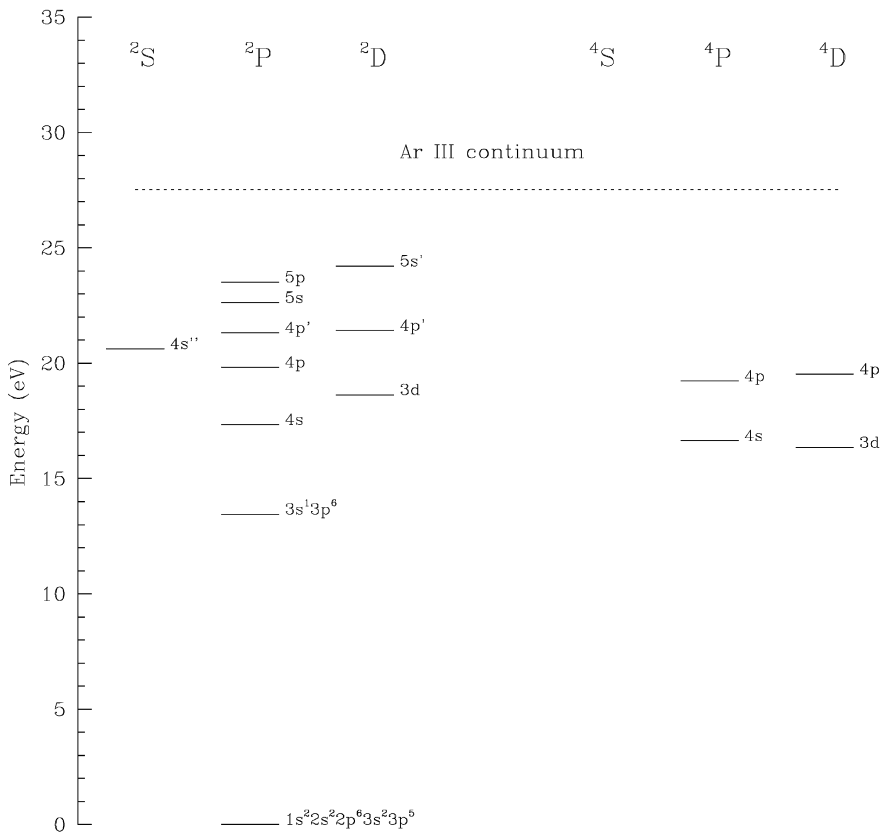


Fig. 2. Partial Grotrian diagram for Ar II configurations that are relevant to the observed emission lines. The energy scale is with respect to the ground state ($3p^5\ ^2P$), which is also shown in the diagram. The core configuration ($3p^4$) can be a 3P state (indicated by the unprimed levels), a 1D state (indicated by the primed levels), or a 1S state (indicated by the double primed level).

The line profile models are based on the Voigt profile formalism for Doppler and Stark broadening,

$$\phi(\nu) = \frac{1}{\pi^{1/2}\Delta\nu_D} H(a, x) \tag{1}$$

$$x \equiv \frac{\nu - \nu_0}{\Delta\nu_D}, \tag{2}$$

$$H(a, x) \equiv \frac{a}{x} \int_{-\infty}^{\infty} \frac{e^{-y^2} dy}{(x - y)^2 + a^2}, \tag{3}$$

where ν_0 is the line-center frequency and $\Delta\nu_D \equiv (2kT_i/m)^{1/2}(\nu_0/c)$ is the Doppler full-width at half-maximum (FWHM). In this expression T_i is the ion temperature and m is the ion mass. The

Voigt parameter, a , is defined as

$$a \equiv \frac{\Gamma}{4\pi\Delta\nu_D}, \tag{4}$$

where Γ is the total damping width (FWHM) including natural and Stark broadening. In the gas cell data, Stark broadening will generally dominate Doppler broadening ($a > 1$) if the ion temperature is close to the electron temperature, which we have deduced is roughly 2 eV [3,5]. In the beam transport plasma it is likely that T_i is comparable to T_e and we consider a model fit with $T_i = T_e$ as a baseline. However, in a pulsed experiment at high ion beam intensity it is difficult to rule out the possibility that T_i could be different from T_e . Consequently, we also consider a model with $T_i = 40$ eV as an example of how high ion temperatures, *if they exist*, affect the results.

The effects of optical depth on the observed multi-line spectrum are included by solving the radiation transfer equation for a uniform medium with no external sources (see for example Ref. [8]). The solution for the intensity is then

$$I_\nu = S_\nu(1 - e^{-\tau_\nu}). \tag{5}$$

The flux can be calculated from

$$F_\nu = 2\pi \int_{-1}^1 I_\nu \mu \, d\mu, \tag{6}$$

where μ is the cosine of the angle between the normal to the detector and the specific intensity vectors. Here S_ν is the source function defined as the ratio of the emissivity, η , to the opacity, κ , and the optical depth, τ , is defined as the integral along the line of sight, z , to the observer of κ , i.e.,

$$\tau \equiv \int_0^l \kappa \, dz = \kappa l \tag{7}$$

for a uniform medium of path length l . The opacity at a given frequency, κ_ν , can be written as

$$\kappa_\nu = n_l \left(1 - \frac{g_l}{g_u} \frac{n_u}{n_l} \right) \left(\frac{\pi e^2}{mc} \right) f_{lu} \phi(\nu). \tag{8}$$

Then using the Boltzmann equation to relate the level populations we find for the optical depth

$$\tau_\nu = n_l (1 - \exp(-\Delta E_{lu}/kT_e)) \left(\frac{\pi e^2}{mc} \right) f_{lu} \phi(\nu) l, \tag{9}$$

where g_l and g_u are the degeneracy of the lower and upper states, respectively, n_l and n_u are the number density of the lower and upper states, respectively, and f_{lu} is the oscillator strength for the bound-bound transition. The f -values and Stark widths are taken from Refs. [6,7] and are listed in Table 1.

The relative optical depths of any two lines can be calculated, assuming that LTE holds among the excited levels, from

$$\frac{\tau_{\nu_1}}{\tau_{\nu_2}} = \frac{g_{l_1}}{g_{l_2}} \exp\left(\frac{-h(\nu_1 - \nu_2)}{kT_e}\right) \left(\frac{1 - \exp(-\Delta E_{lu_1}/kT_e)}{1 - \exp(-\Delta E_{lu_2}/kT_e)} \right) \frac{f_1 \phi_1(\nu)}{f_2 \phi_2(\nu)}. \tag{10}$$

All of the variables in this equation are known atomic parameters, except for the line profiles and the electron temperature. If we ignore differences in the line profiles, then the ratio of the line optical depths is dependent only on the electron temperature. The electron temperature is known from the measurements and calculations described in Ref. [3], which also show that LTE is reached by about 10 ns, which is the earliest time for which we analyze spectra in this paper. The *relative* optical depths are thus determined in this way from the value for a single reference line. We chose the $4s\ ^4P_{5/2} - 4s\ ^4D_{7/2}$ transition at 4348 Å as the reference line. Therefore, the only free parameters of interest for a model at a given T_e are the electron density, the optical depth of the 4348 Å line.

In addition to the Stark and Doppler broadening and the effects of opacity, we include instrumental broadening in our spectral model via a convolution of the synthetic spectra with a Gaussian, representing the instrumental function. The width of this instrumental profile was determined from a laser fiducial line recorded on the spectrograph. We found that the specific value chosen for the instrumental FWHM within the range of uncertainty of the fiducial line measurement did not affect the derived model parameters.

The model fitting, which is described in detail below, showed that varying the electron temperature between 2 and 3 eV, which is the range indicated by the Boltzmann plot analysis [5], did not affect the line profiles through Doppler broadening. Its effect on the line ratios via the level populations was quite modest, and so we fixed the electron temperature for all models at 2 eV, varying only the electron density, n_e , and the 4348 Å optical depth, τ_{4348} , which in turn controlled the values of the other line optical depths.

From the governing equation for the spectral emission lines (Eq. (6)), we calculated synthetic spectra and compared them to the data. The goodness of fit was assessed using the χ^2 statistic, given by

$$\chi^2 = \sum_i^N \frac{(x_i - m_i)^2}{\sigma_i^2}, \quad (11)$$

where N is the number of data points, x_i are the data, σ_i are the statistical uncertainties on the data, and m_i are the model fluxes. The uncertainties were calculated by converting the recorded intensities to photoelectron counts, and using experimentally verified Poisson statistics [9]. The model fluxes were adjusted to compensate for the measured spectrograph efficiency as a function of wavelength. We allowed the free parameters, n_e and τ_{4348} , to vary and found local χ^2 minima using the Levenberg–Markwardt method, as implemented in Ref. [10]. We randomly perturbed the parameters once a local minimum was found, and considered the deepest local minimum to be the global minimum once 200 unsuccessful attempts were made to find deeper minima by this method. The model parameters that gave this global χ^2 minimum were thus determined to be the best-fit parameters.

In order to assign formal uncertainties to these parameter values, we calculated a series of synthetic spectra and their attendant χ^2 values on a grid that spanned the $(n_e - \tau_{4348})$ parameter space. Then for each point in parameter space, we formed the $\Delta\chi^2 = \chi^2 - \chi_{\min}^2$ statistic, which defines the confidence limits as described in Ref. [11]. A given confidence limit on the range of parameters corresponds to a specific $\Delta\chi^2$ criterion. For two free parameters of interest, the 95.4% confidence limit, for example, is given by $\Delta\chi^2 = 6.2$. We note again that the formal uncertainties

used in the calculation of the χ^2 values are statistical errors only (i.e. systematic uncertainties due, for example, to approximations in the spectral model, are not included).

For each 3 ns lineout considered, we subtracted the contribution from the continuum before fitting the emission lines. We fit and subtracted several different continuum models represented by polynomials of varying degrees. We found that the specific continuum model had very little effect on the derived parameters. In some cases, unidentified blends compelled us to exclude points on the wings of a given line. We conclude by noting that the line-center wavelengths in the data were determined separately before we commenced the model fitting described in this section. This step was performed in order to account for any errors in the wavelength scale of the spectra.

4. Results of model fitting

Here we present the results of our fitting analysis on five lineouts from PBFA-II experiment number 6022, taken between 10 and 22 ns after the introduction of the beam into the gas cell. The data are shown in Fig. 3, along with the best fit model, which is discussed below. As we described in the previous section, the only two free parameters are the electron density and the optical depth of the reference line at 4348 Å. However, because of uncertainty about the actual value of the ion temperature, we fit two different families of models. In the first case, we assume $T_i = T_e = 2$ eV, and in the second case we assume $T_i = 40$ eV (and $T_e = 2$ eV).

It is possible that the ion temperature exceeds the electron temperature during the time these data were taken. The electron equilibration time should be short, but the timescale for the ions to come into temperature equilibrium with the electrons is expected to be relatively long (approximately 80 ns for a plasma density of 10^{17} cm⁻³ and $T_e = 2$ eV and $T_i = 40$ eV). It turns out that the derived best-fit electron densities and optical depths vary by less than a factor of two (and generally much less) between these different temperature cases. The fit qualities are comparable, and we cannot statistically distinguish between the two cases. We can, however, rule out ion temperatures as high as 100 eV. Such models lead to unacceptably high χ^2 values. In the remainder of this section, we consider the nominal model, with $T_i = T_e = 2$ eV.

In Table 2 we list the results of fitting the synthetic spectra to the data. The best-fit parameter values are shown, along with the corresponding reduced- χ^2 values, $\chi_v^2 = 1/\nu\chi^2$, where $\nu = (N - p)$ is the number of degrees of freedom, given by the number of data points minus the number of free parameters. Uncertainties on the parameter values (n_e and τ_{4348}) are taken from the maximum extent of the 68.3% confidence limits.

The confidence limits in the plane of the fitted parameters for the five data sets are shown in Fig. 4. This figure demonstrates that the largest reasonable optical depths are obtained in models with low electron densities, and vice versa. This is understandable because the actual line widths are fixed and some combination of the two primary broadening mechanisms must contribute to them. If, for example, opacity effects account for the majority of the line width, then Stark broadening can account for very little of it.

The fits to the data are generally adequate, but not ideal, as is demonstrated by the χ_v^2 values listed in Table 2 which tend to be somewhat greater than unity. The quality of the fits can also be seen by comparing the data to the best fit spectral model in Fig. 3. The formal

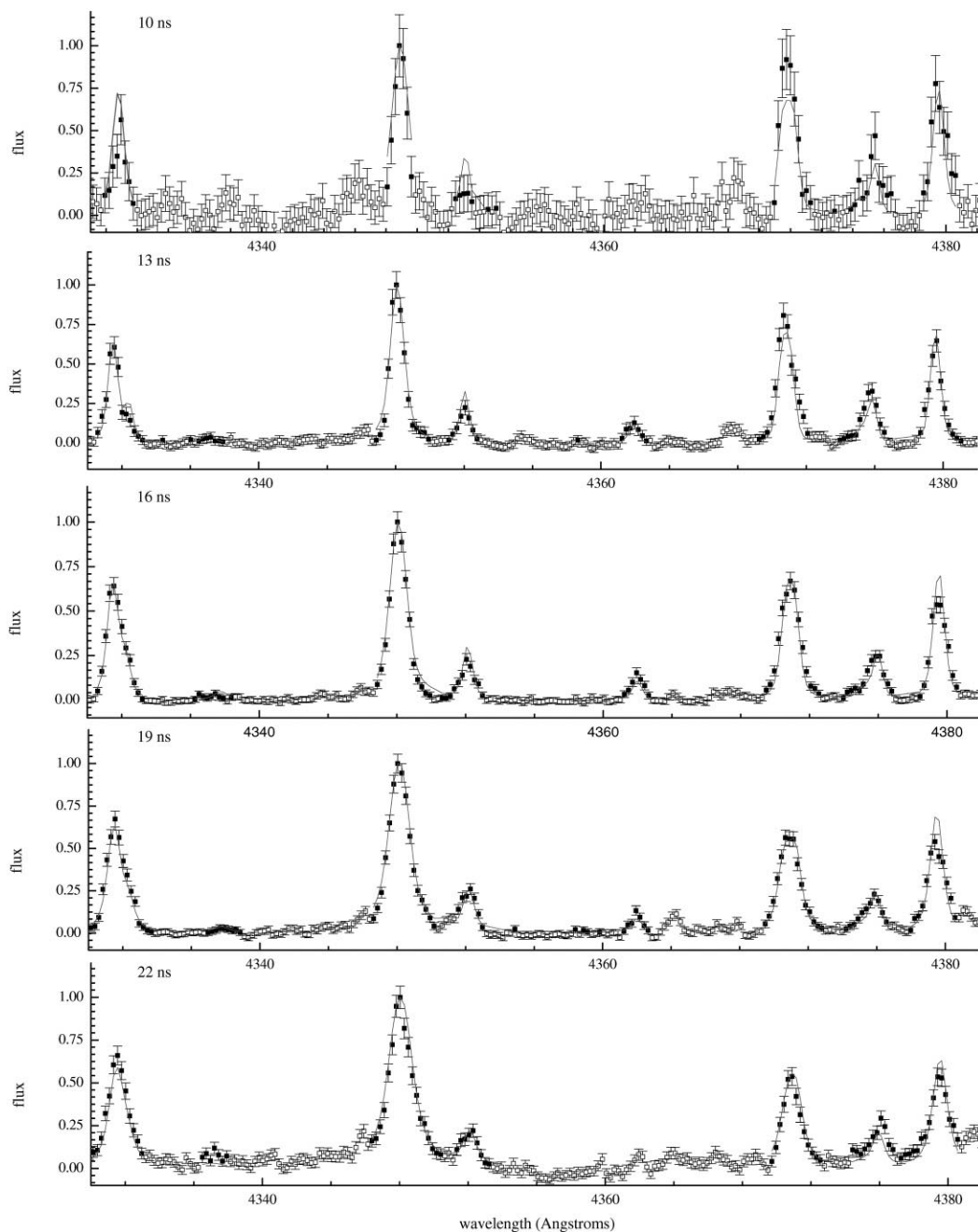


Fig. 3. For the five lineouts, we show the data (filled squares) included in the analysis along with the best-fit optically thick model, with $T_i = T_e = 2$ eV (red lines). Note that the displayed data are normalized to that the intensity of the 4348 Å line is defined as unity in each lineout. This normalization is for display purposes; the fitting was carried out with the data in count units.

Table 2
Fitted model parameters

Time (ns)	χ^2_v	n_e (10^{17} cm^{-3})	τ_{4348}	τ_{4352}	τ_{4362}	τ_{4376}	τ_{4380}
10	1.0	$0.55^{+0.22}_{-0.19}$	$26.6^{+19.4}_{-8.6}$	1.3	0.4	0.9	5.3
13	1.5	$0.39^{+0.07}_{-0.06}$	$27.3^{+5.8}_{-4.7}$	1.4	0.4	0.9	5.5
16	2.4	$0.67^{+0.05}_{-0.07}$	$19.1^{+3.1}_{-1.7}$	1.0	0.3	0.6	3.8
19	1.6	$1.15^{+0.06}_{-0.12}$	$11.7^{+1.8}_{-0.9}$	0.6	0.2	0.4	2.3
22	1.6	$1.68^{+0.13}_{-0.14}$	$8.0^{+1.0}_{-0.8}$	0.4	0.1	0.3	1.7

uncertainties, which are entirely statistical, are quite small for these data (with the exception of the first lineout). Thus the χ^2_v values somewhat above unity arise from systematic errors which are not accounted for in the formal uncertainties. Such systematic errors could be due to uncertainties in the atomic physics (f -values or Stark widths), plasma gradients or inhomogeneities, uncertainties in the calibration of the spectrograph sensitivity, or problems with the continuum subtraction.

For comparison, we also show the spectrum at 13 ns with the best-fit *optically thin* model in Fig. 5. The fit is obviously poor ($\chi^2_v \approx 9$). With the 4348 Å line flux forced to agree with the data in the model fit, the intensities of the weaker lines are consequently underestimated. It is only when the optical depth is included that the relative intensities of the weaker lines increase to the values seen in the data. Additionally, this optically thin model overestimates the Stark broadening and thus the electron density. This can be seen in strong wings (relative to the weak line-center intensities) of the weaker lines in the model. In none of the five lineouts does an optically thin model lead to a good fit, providing strong evidence for the importance of optical depth effects in the argon gas cell in these experiments.

We have also compared the time-evolution of the electron density and temperature derived from the five lineouts with the results of the detailed collisional-radiative modeling, previously mentioned in Section 2. This modeling effort is fully described in Ref. [5], and can be summarized as a time-dependent non-LTE calculation of over 500 Ar levels, taking into account beam-impact and hot-electron collisional processes as well as thermal processes. The non-thermal processes cause direct ionization/excitation from the Ar I ground state initially, favoring the population of the doublet levels. Later, collisions with thermal electrons control the relative populations of the different terms within and among these Ar II excited levels. The time dependence of the different Ar II lines intensities in the first 10 ns confirm this scenario [3]. The time-dependent electron densities and 4348 Å optical depths from these calculations are shown in Fig. 6 for $T_e = 2, 2.5,$ and 3 eV , along with the values we derived from the data. For both the optical depth and the electron density, the values derived from the data lie between those predicted by the $T_e = 2.5 \text{ eV}$ model and the $T_e = 3 \text{ eV}$ model.

We should also note that the final electron density data point is somewhat higher than the models predict. This may be due to impurity electrons, possibly from the gas cell container, that appear at late times, but are not included in the models. Another possible cause of this deviation—and also of the mild disagreement (see Fig. 6) between the optical depth and electron density data in terms of the different temperature models—is the presence of gradients in

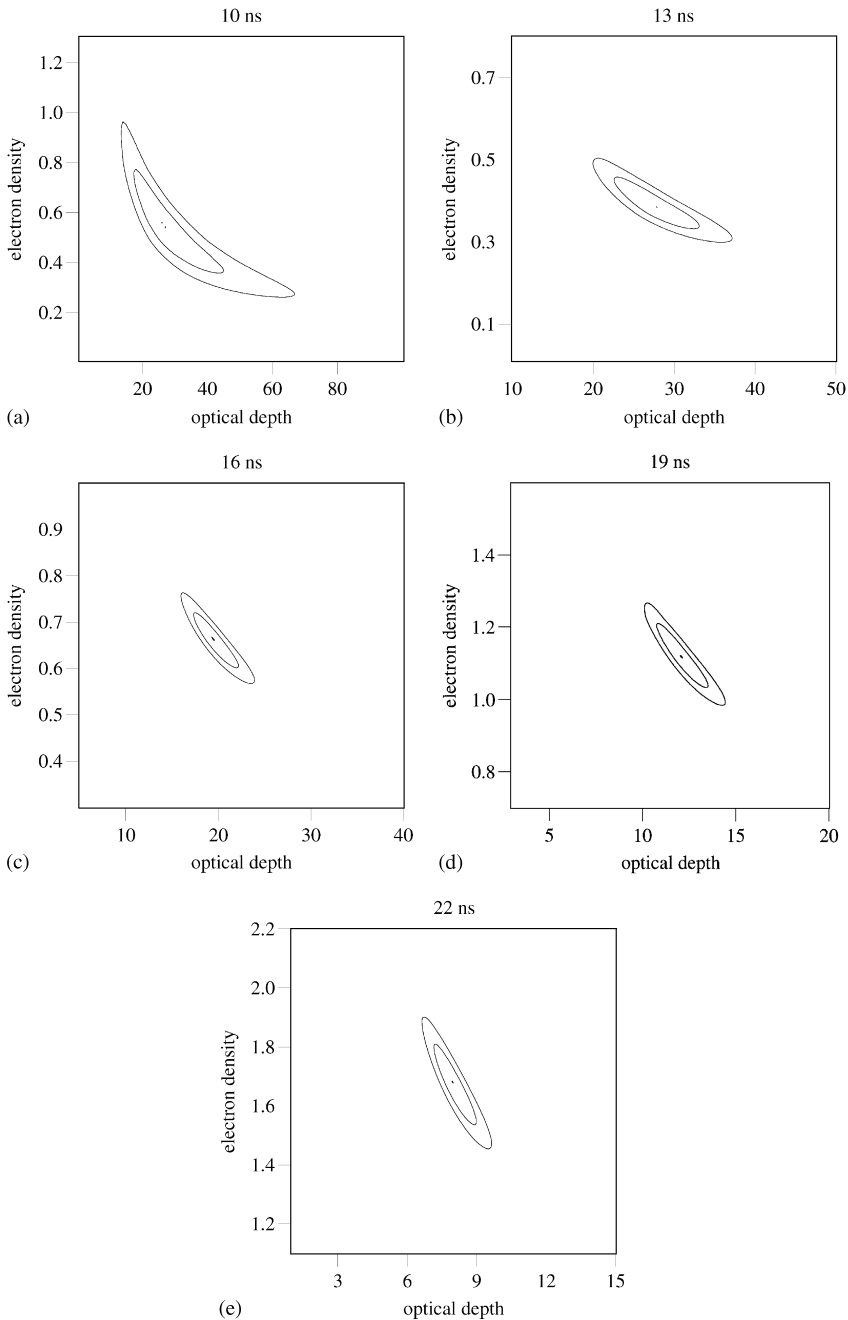


Fig. 4. For the five lineouts, we show the best fits and the 68.3 and 95.4% confidence limits in the n_e - τ_{4348} plane.

the emitting plasma. Both our spectral model and the detailed models described in Ref. [5] assume a uniform plasma. However, there will be radial temperature and density gradients due to the influence of the beam ions, which are concentrated in a narrow, pinched region. For the optically thick lines, the spectrometer will not see as far into the beam region, and so the emission

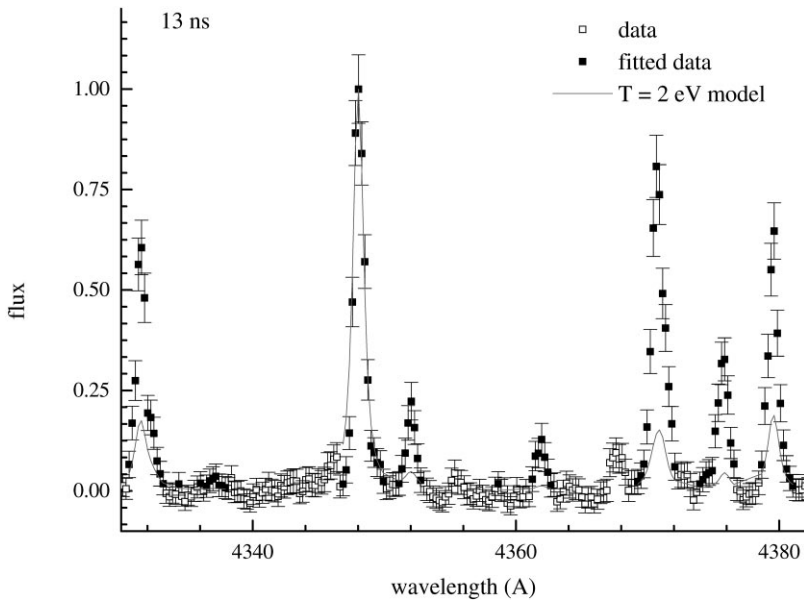


Fig. 5. The data from the 13 ns lineout shown with the best-fit optically *thin* model.

lines may, to some extent, be sampling conditions in different physical locations. We note however, that temperature gradients cannot be severe because central self-reversals are not seen in any emission lines.

Finally, we will briefly mention two consistency checks of the multi-line fitting procedure. The first is to determine the electron density by fitting an individual optically thin line that has a relatively large Stark width. For example, the 4337 Å line arises from a $5s' \ ^2D_{3/2}$ excited state that is 24.29 eV above ground. This is relatively high-lying compared to the other lines and the 4337 Å line consequently has larger Stark broadening. This line is also optically thin according to the multi-line fitting results. We therefore fit the 4337 Å line individually and found 1σ ranges in the derived electron density value for each lineout that were consistent with the best-fit values from the multi-line fitting. This range for the 4337 Å line was in all cases larger than the extent of the 68.3% confidence limits on the models fit to the ensemble of lines, which was probably due to the relatively poor signal-to-noise of the line in question. Indeed, it is one of the powerful properties of the multi-line fitting technique that by using many lines, the overall effective signal-to-noise of the data can be very high, even when that of individual lines is low.

The second consistency check provided an additional way of evaluating whether Stark broadening dominates Doppler broadening in these data. It relies on examining the ratio of widths for two optically thin lines with different Stark broadening. For example, the 4337 and 4352 Å lines are both optically thin and they both have the same Doppler broadening, but the 4337 Å line has a Stark width that is approximately 2.2 times larger. Thus, if Stark broadening dominates over Doppler, the 4337 Å line width should be significantly larger than the 4352 Å line width. Assuming a Voigt profile, at $T_i = 1 \text{ eV}$ (where the Voigt parameter, a , is 10 and 5 for the two lines, respectively,

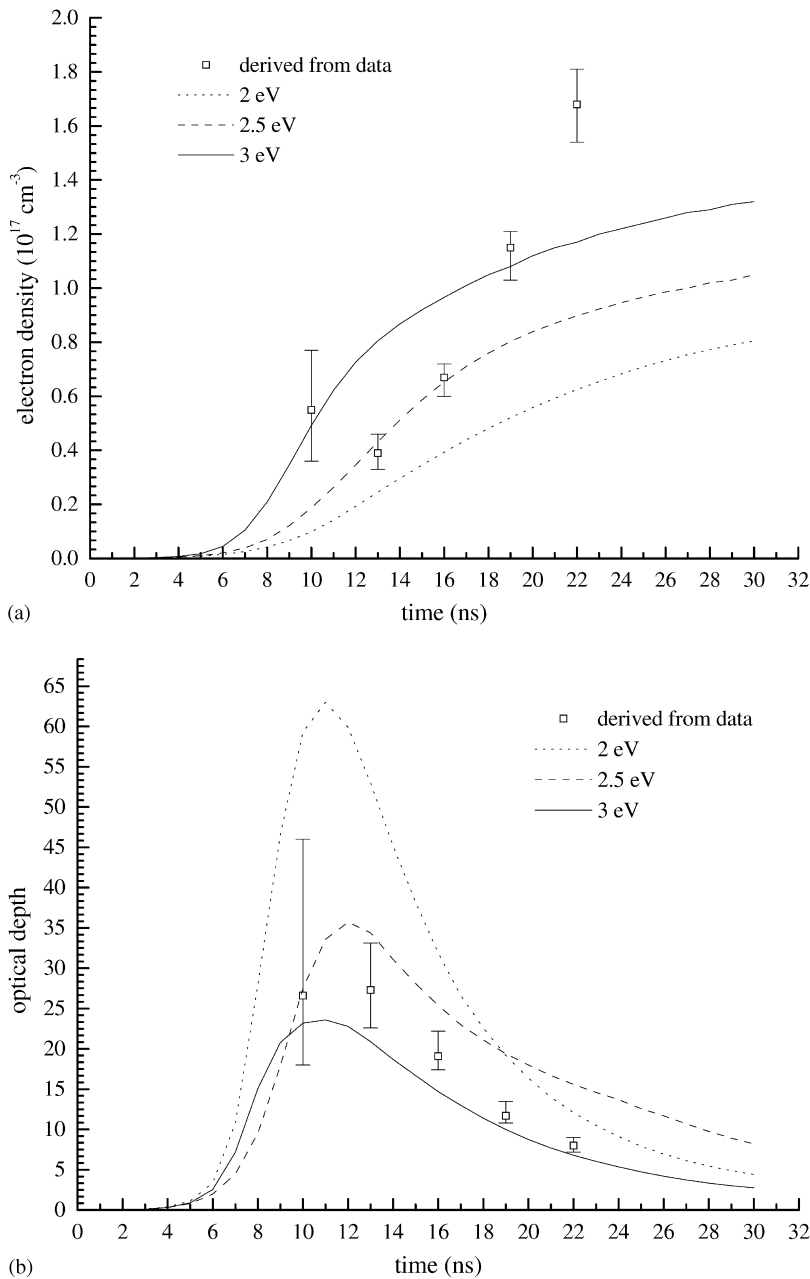


Fig. 6. The derived electron density (a) and optical depth (b) value for the five fiducial times, shown with profiles from time-dependent modeling [5]. The models are calculated for three different temperatures.

at $n_e = 10^{17} \text{ cm}^{-3}$, the ratio of widths is expected to be $4337/4352 = 1.94$. At $T_i = 100 \text{ eV}$ (where the Voigt parameters are much less than unity), the ratio is predicted to be 1.31. When we deconvolve the instrumental profile for these lines, determine the widths of the two lines in each of the five lineouts, and then average the widths over the five lineouts, we find an average line-width

ratio of $4337/4352 = 2.43 \pm 1.08$. This is consistent with the lower-temperature model in which Stark broadening dominates Doppler broadening.

5. Conclusions

We have demonstrated a useful and powerful method for deriving information about plasma conditions from a multi-line spectrum in which both opacity and Stark broadening are important. The method is useful because it provides a quantitative way to assess uncertainties on the fitted model parameters. The method is powerful due to its use of a large number of emission lines, and to the requirement that a single model fit all of the data simultaneously. In fact, the inclusion of weak lines adds to the constraints on the model parameters.

As applied to the argon gas cell spectra in intense light ion beam experiments at PBFA-II, the fitting procedure demonstrates the importance of the inclusion of optical depth effects in modeling emission line spectra. The combined Stark- and opacity-broadened LTE model provided good fits to the data at all times between 10 and 22 ns, and these values have been compared to detailed time-dependent models of the ionization dynamics in the gas cell.

Our treatment of line optical depth effects, and the resulting derived electron densities and optical depths, significantly improve the consistency among several aspects of these ion beam gas cell experiments. First, in Ref. [3], the plasma electron temperature was determined using a Boltzmann plot analysis. The standard deviation of the fits used in that analysis were found to be greatly reduced when an optically thick treatment of the lines was used. The bounds on the opacity determined in that analysis were consistent with the opacities determined in this work. In addition, the spectral fits to the Ar II lines are much improved when we assumed finite optical thickness (compare Figs. 3 and 5). Also, the ionization dynamics from the detailed modeling [5] agree when the data are interpreted using a finite optical depth model, as opposed to an optically thin model. Finally, the absolute level populations from the detailed calculations are in good agreement with the time-dependent 4348 Å optical depths we derive in our fitting analysis. The consistency among all of these factors argues strongly that our adopted model, which includes optical depth effects as well as Stark and Doppler broadening, provides an accurate description of the physical conditions in the PBFA-II ion beam gas cell.

In conclusion, we note that this joint-probability spectral fitting method is applicable generally. Confidence limits can be reliably placed on the parameter values of multi-parameter spectral models using the $\Delta\chi^2$ statistic for a wide variety of models.

References

- [1] Kilkenny JD, Lee RW, Key MH, Lunney JG. *Phys Rev A* 1980;22:2746.
- [2] Kastner SO, Bhatia AK. *JQSRT* 1997;58:217.
- [3] Bailey JE, Chung H-K, Carlson AL, Cohen D, Johnson DJ, Lake P, MacFarlane JJ, Wang P, Welch D. *Phys Rev Lett* 1999;82:739.
- [4] Van Devender JP, Bluhm HJ. In: Vellarde G, Ronen Y, Martinez-Val JM, editors. *Nuclear fusion by inertial, confinement*, Ann Arbor: CRC Press, 1993, p. 455.
- [5] Chung H-K, MacFarlane JJ, Wang P, Moses GA, Bailey JE, Olson CL, Welch DR. *Rev Sci Inst* 1997;68:350.

- [6] Pellerin S, Musiol K, Chapelle J. *JQSRT* 1997;57:359.
- [7] Pellerin S, Musiol K, Chapelle J. *JQSRT* 1997;57:377.
- [8] Mihalas D. *Stellar atmospheres* (2nd ed.). San Francisco: Freeman, 1978.
- [9] Bailey JE, Adams R, Carlson AL, Ching CH, Filuk AB, Lake P. *Rev Sci Inst* 1997;68:1009.
- [10] Press WH, Flannery BP, Teukolsky SA, Vetterling WT. *Numerical recipes*. Cambridge: Cambridge University, 1991 (Chapter 14).
- [11] Lampton M, Margon B, Bowyer S. *Astrophys J* 1976;208:177.